RSC Advances

PAPER

View Article Online
View Journal | View Issue

Cite this: *RSC Adv.*, 2023, **13**, 28224

Directional design of carboxylic acid coordination number fine-tuned space structure to improve the output performance of nanogenerators†

Yong-Juan Zhou,[b] Shi-Hui Wang,[b] Zi-Kun Zhang[b] and Jiabin Xiong *[ab]

The emergence of nanogenerators, which provide a way to obtain mechanical energy from the environment and to collect and transmit tiny amounts of energy, has attracted a lot of attention. MOFs, because of their diverse structures as well as stable pores and large specific surface area, have very significant advantages to be used as nanogenerator materials. In this paper, two MOFs with similar spatial structures are designed to take advantage of the different coordination numbers of carboxylic acids to achieve the regulation of their microstructures. The output performance of friction power generation was found to be affected significantly by their microstructures. The friction power generation performance improved with the increase of carboxylic acids, and the obtained polyacid ligand materials can be used for light bulb illumination, which is a step forward for the practical exploration.

Received 6th August 2023
Accepted 17th September 2023

DOI: 10.1039/d3ra05327j

rsc.li/rsc-advances

Introduction

As people pay attention to environmental pollution, new energy technologies are developing rapidly. Solar, wind and other sustainable energy sources have a positive impact on environmental protection.[1,2] However, most of them are still costly compared to fossil fuels and constrained by various factors,[3] which has prevented them from being popularized on a large scale. In 2012, Prof Zhonglin Wang and his team invented the TENG, which works through the coupling of the friction electric effect (contact charging) and electrostatic induction.[4–6] The kinetic energy generated by human mechanical movements in daily life, such as limb movements, heartbeat and breathing, can be converted into electrical energy and electrostatic induction based on the friction electric nanogenerator (TENG). The electrical energy converted by TENGs can be applied to self-powered sensors,[7–13] drug delivery,[14–17] wearable electronic devices,[18–20] self-powered electrochemical cathodic protection,[21–25] batteries and supercapacitors.[26,27] Among the nanogenerators, friction electric nanogenerators (TENGs) have attracted attention due to their high output and high energy conversion efficiency.

There are two ways to increase the output performance of TENGs, one is to increase the charge density,[28] the other is to reduce the charge loss.[29] MOF (metal organic framework) materials have many excellent properties[30,31] and are being considered for use as friction nanogenerator materials. MOFs have functional frameworks and open channels, which provide multiple high-speed carrier-ion (electrons, holes, and ions) transport paths, avoiding the pitfalls of large internal resistances and small output currents. Improving the charge density can be achieved by increasing the contact area, the increase in the porous structure of MOFs leads to an increase in the pore diameter, which increases the effective contact area of the material, and the holes cause more charge traps to absorb electrons, creating more charge density and resulting in a TENG with high output properties. The effect of ligand side chain differences on the performance of TENGs with similar spatial structures of the materials was not well understood in literature. Deep investigations on the relationship between structure and performance are still in great needs. Those investigations could provide a guide line for the development of high performance TENGs based on metal–organic skeleton.

In this paper, we selected compounds generated by the reaction of metals Zn and Cu centered on ligands 1,1,2,2-tetrakis(4-carboxylic acid biphenyl)ethylene (H_4TCPE)[32] and tetrakis[4-(3,5-dicarboxylic acid phenyl)]tetraphenylethylene (H_8ETTB)[33] with different spatial structures as friction nanogeneration materials for the preparation of TENGs (respectively, referred to as compounds **1** and **2**), and the prepared Zn-MOF-TENG devices were named 1-TENG and Cu-MOF-TENG devices were named 2-TENG. The electrochemical characterization test results show that compound 2-TENG has the best output performance, followed by **1**-TENG. We have shown that

[a]*College of Chemistry, Green Catalysis Center, International Phosphorus Laboratory, International Joint Research Laboratory for Functional Organophosphorus Materials of Henan Province, Zhengzhou University, Zhengzhou 450001, China. E-mail: xjiabin@foxmail.com*

[b]*School of Material and Chemical Engineering, Center for Advanced Materials Research, Zhongyuan University of Technology, Zhengzhou 450007, China*

† Electronic supplementary information (ESI) available. See DOI: https://doi.org/10.1039/d3ra05327j

the increase in the end carboxylic acid structure, more uniform refinement of the cavity structure, improving the cavity current-carrying efficiency, and the increase in electronegativity further improves the friction power generation output performance, thus obtaining a high-output performance material. Furthermore, in order to prove its good performance, we applied it to light up a small light bulb.

Experimental

Compounds preparation

The chemicals and reagents involved in this experiment were obtained by purchasing through commercial platforms and were used directly without further purification. Both compounds **1** and **2** (ref. 32 and 33) were prepared according to the reported literature. The compounds were subjected to Mott–Schottky test by a three-electrode system on an electrochemical workstation (CHI 660E, Shanghai Chenhua Instrument Co., Ltd., China). The crystal structure is determined by X-ray single crystal diffractometer, and the crystal structure can be solved. The single crystal structure was mapped by Diamond Software.

Synthesis of $[Zn(HTCPE)]_n$ (compound 1)

$Zn(NO_3)_2$–$6H_2O$ (16.06 mg, 0.054 mmol), H_4TCPE (8 mg, 0.009 mmol) and 4,4′-bipyridine (3 mg, 0.017 mmol) were dissolved in a mixture of methanol (0.5 mL), DMF (2 mL), and 10 μL (1 M) hydrochloric acid. The mixed solution was then placed in a 10 mL reactor and heated in a programmable oven that was preheated to 110 °C for 48 h, and then cooled to room temperature at a rate of 5 °C h^{-1} to obtain light yellow Zn-MOF [Zn(HTCPE)] crystals. These crystals obtained were washed with excess DMF and methanol and dried at room temperature.

Synthesis of $[Cu_4(ETTB)]_n$ (compound 2)

$Zn(NO_3)_2$–$6H_2O$ (15 mg) was dissolved with H_8ETTB (5 mg) in a solution of *N*,*N*-diethylformamide (1.6 mL), and the resulting mixed solution was placed in a 5 mL heat-resistant vial, followed by the addition of 1 drop of fluoboric acid. The mixed solution was placed in an oven preheated to 75 °C for 96 h and then cooled to room temperature at a rate of 5 °C h^{-1} to obtain colorless Zn-MOF [Zn(H_8ETTB)] crystals. The Zn-MOF [Zn(H_8-ETTB)] crystals were washed with appropriate amount of DMF and methanol and dried at room temperature. Colorless crystals of Zn(H_8ETTB) (5 mg) and $Cu(NO_3)_2$ $2.5H_2O$ (15 mg) were taken and added to 1.6 mL of *N*,*N*-dimethylformamide, and the resulting mixture was placed in a 5 mL heat-resistant vial, and the mixture was stored at room temperature for 4 days to obtain green crystals of $[Cu_4(ETTB)]$. The obtained green crystals were washed with excess DMF and methanol and dried at room temperature.

Results and discussion

Compound **2** was synthesized in two main steps. It was first synthesized from the metal Zn and H_8ETTB by solvothermal method, and then Zn was substituted with Cu at room temperature. The crystal structures of the compounds are shown in Fig. 1. In compound **2**, all four coordination bonds of the central metal Cu ion are coordinated to the oxygen atom in the carboxylic acid (Fig. 1a). One of the oxygen atoms is from one carboxylic acid of each of the four ligands, and the oxygen atoms in the bicarboxylic acid at the end of the ligand are each linked to two Cu ions (Fig. 1b). Fig. 1b–d show the crystal structures of the compounds along the *a*-axis, *b*-axis, and *c*-axis, respectively. C, grey; O, red; Zn, blue; and H, white. From the figure, it is quite obvious that the compounds are rhombic coordination polymers.

The compounds were tested for characterization by PXRD, FT-IR and XPS. The PXRD patterns tested for compound **2** were in agreement with the reported PXRD patterns, indicating a good compound fit (Fig. 2a), which ensured good crystallinity and purity of the compounds. The ionic valence and elemental composition of the metals in the compounds were analyzed by XPS test.

As can be obtained from Fig. 2b and S2,† the characteristic peaks at 1655 cm^{-1} of the IR spectrum are the C=O double bond stretching vibration peaks of compounds **2**, **1**. Among them, the characteristic peak at 773 cm^{-1} in Fig. 2b is the single-substituted CH out-of-plane bending vibration peak of the benzene ring of compound **2**, and in Fig. S2,† the characteristic peak at 783 cm^{-1} is the interstitial double-substituted CH out-of-plane bending vibration peak of the benzene ring of compound **2**. The XPS full spectrum of compound **1** showed that the compound contained Zn, C, N, O elements (Fig. S3a†). The XPS full spectrum of compound **2** indicates that it contains Cu, C, N, O, Zn elements, with 75% of the Zn found to be displaced by EDS (Fig. 2c and S13†). Fig. S3b† and 2d show the energy level analysis of compounds **1** and **2** for 2p of metal elements, respectively. The peaks at 1022.25 eV and 1045.40 eV in Fig. S3a† correspond to Zn^{2+} $2p_{3/2}$ and $2p_{1/2}$, respectively; the peaks at 933.68 eV and 953.48 eV in Fig. 2d correspond to Cu^{2+} $2p_{3/2}$ and $2p_{1/2}$, respectively.

Fig. S4† shows the thermogravimetric analysis (TGA) curves and N_2 adsorption–desorption isotherms of compounds **1** and **2** after drying at room temperature. Compounds **1** and **2** showed

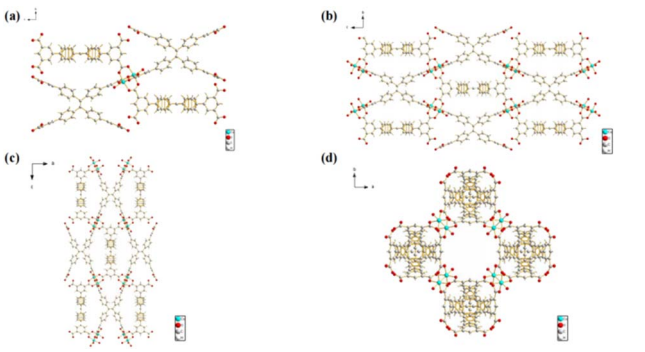

Fig. 1 Perspective view of the crystal structure of Cu-MOF (a) complex structure of the Cu-metal node (b) crystal structure of Cu-MOF along the crystallographic *a*-axis, (c) *b*-axis, and (d) *c*-axis. C, gray; O, red; Zn, blue; H, white.

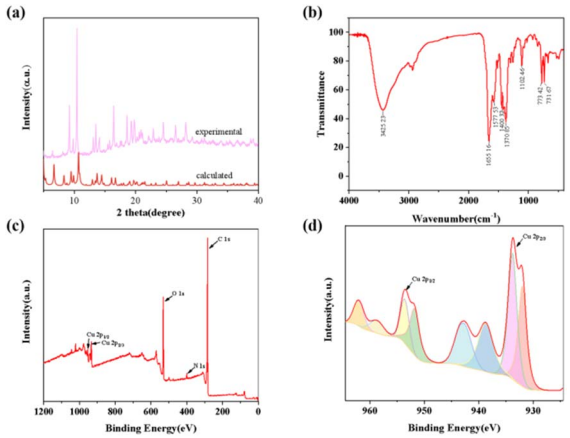

Fig. 2 (a) XRD; (b) FT-IR; (c) XPS full spectrum; (d) Cu ion XPS profile of compound **2**.

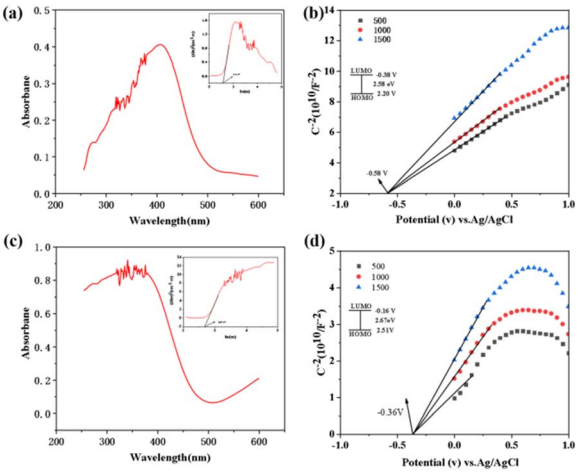

Fig. 3 (a and c) UV-vis diffuse reflectance spectra of compounds **1–2** (the insets in the upper right corner are the corresponding Tauc plots, respectively); (b and d) Mott–Schottky of compounds **1–2** tested in 0.2 M Na_2SO_4 solution.

significant weight loss at 392 and 272 °C, respectively, which corresponds to the literature. The BET specific surface area of compounds **1** and **2** were 79.27 $m^2\ g^{-1}$ and 217.43.00 $m^2\ g^{-1}$, and the adsorption–desorption values were 82.23 $cm^3\ g^{-1}$ and 182.64 $cm^3\ g^{-1}$ respectively, which were type IV adsorption–desorption isotherms, and the pore size distribution curves indicated the presence of mesopores in the materials.

Compounds **1–2** were synthesized from different metal ions (Zn, Cu) with different ligand structures. Since the metal centers have less influence on their properties,[34] and as the crystallographic data of the compounds show that the structures of the two compounds differ greatly (Table S1†), we mainly discuss the influence of their structures on the output properties of TENG. When the difference between the electron-giving and electron-harvesting abilities of the pair of electrode materials of the friction nanogenerator is larger, the charge migration between the electrodes will be larger and the output performance of the TENG will be better. Since a negative charge on the hydroxyl oxygen in the carboxylate anion can apportion a portion of the required negative charge density on the carbonyl oxygen, reducing its electron-withdrawing induced effect and making the electron-withdrawing ability weaker, the more carboxylic acids there are, the better the performance of its TENG.

Mott–Schottky test and UV-2600 spectroscopic test were performed for compounds **1** and **2** (Fig. 3). The Mott–Schottky test allows us to determine the semiconductor type of the compounds as well as the size of the highest occupied orbital (HOMO) and the lowest unoccupied molecular orbital (LUMO) to prejudge the corresponding TENG output performance. The UV-vis diffuse reflectance spectra of compounds **1** and **2** are shown in Fig. 3a and c, respectively, and their insets are the corresponding Tauc plots, from which the bandgap energies (E_g) of compounds **1** and **2** are found to be about 2.58 eV and 2.67 eV, respectively. From the positive slopes of the Mott–Schottky plots (Fig. 3b and d) *versus* the potential curves, it is found that compounds **1** and **2** are both n-type semiconductors, compounds **1** and **2** have LUMO orbitals of −0.38 V and −0.16 V (obtained at −0.58 V and −0.36 V bonding, respectively) and HOMO orbitals of 2.20 eV and 2.50 eV for **1** and **2**, respectively, for the value of Ag/AgCl as a reference. It can be concluded that the HOMO orbitals of compound **2** are slightly higher than the HOMO orbitals, indicating that compound **2** has a stronger internal electron-leaping ability and higher output performance, so we guess that the output performance of **2**-TENG will be slightly better than that of **1**-TENG.

The working principle of TENG based on MOF materials is based on the coupling of friction charging and electrostatic induction. In this experiment, the simplest vertical contact-detachment mode (Fig. S5†) is used, in which a pair of friction electric layers made of materials with different electron affinities are physically contacted to generate friction charges; triggered by an external mechanical force, the relative motion between the friction electric layers disrupts the equilibrium electrostatic charge distribution on the electrodes; the potential difference between the electrodes is established, and the free electrons flow through the external circuits in order to reach a new equilibrium, and when the friction electric layer moves

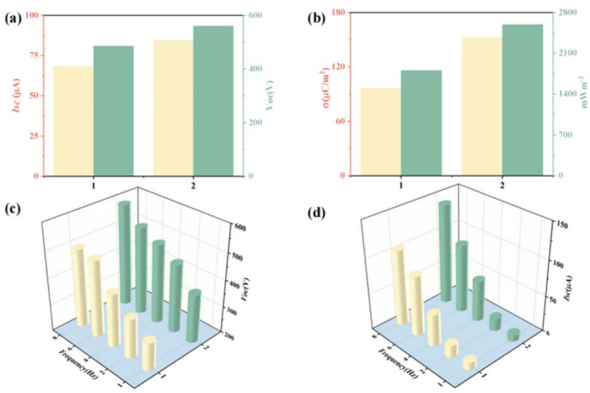

Fig. 4 Comparison of (a) current–voltage, (b) charge power density, (c) different Hz currents, (d) different Hz voltages for compounds **1–2**.

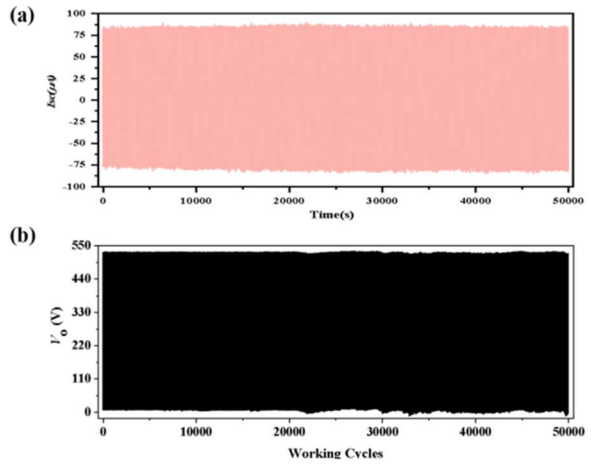

Fig. 5 2-TENG after 50 000 cycles of (a) I_{sc}; (b) V_{oc}.

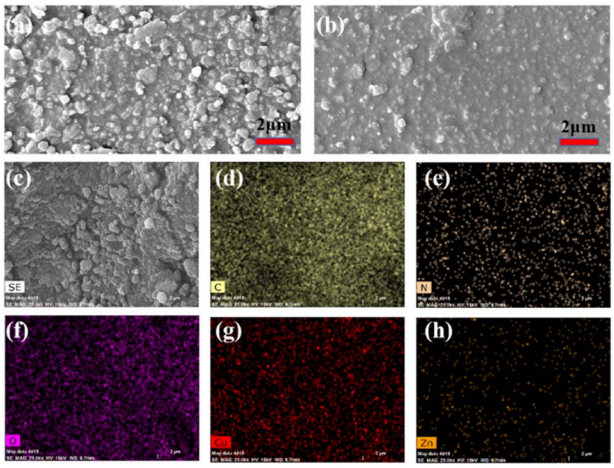

Fig. 6 (a) FE-SEM image of compound 2 before testing; (b) SEM image of compound 2 after testing; (c–h) EDX-mapping analysis of each element in compound 2.

backward, the free electron flow returns to the original electrostatic equilibrium.[35–38]

The friction power generators 1-TENG and 2-TENG were fabricated by using compounds 1 and 2 as positive electrode materials and polyvinylidene fluoride (PVDF) as negative electrode material, respectively. Under the same experimental conditions, the short-circuit currents and open-circuit voltages of the 1- and 2-TENGs at a frequency of 5 Hz reached 68.23 μA and 485.32 V, 84.49 μA and 560.45 V (Fig. 4a). From the output performance of the TENG, it can be found that the I_{sc} and V_{oc} of the 2-TENG are larger at 5 Hz. The charge density (σ) is also a fundamental parameter to evaluate the performance of TENG. The charge densities of 1- and 2-TENG at 5 Hz were calculated to be 96.24 μC m^{-2} and 151.99 μC m^{-2}, respectively. The power density was calculated by collecting the short-circuit currents of the TENG with different load resistances, and it was found that the instantaneous power reaches its peak value when the load resistance is 10 MΩ, which is 1806.36 mW m^{-2} and 2594.93 mW m^{-2} respectively (Fig. 4b), and it is obvious that 2-TENG has a greater charge density *versus* power density. In addition, we also tested the output performance of compounds 1, 2 at different frequencies and found that I_{sc} (Fig. 4c) and V_{oc} (Fig. 4d) increase with the increase of frequency, and the output performance of 2-TENG is significantly higher than that of 1-TENG at 1–8 Hz. When 1-TENG is operated at 8 Hz, the current and voltage reach 105.86 μA and 493.90 V, while 2-TENG can reach as high as 140.35 μA and 583.48 V at 8 Hz. All these test results demonstrate that the output performance of 2-TENG is greater than that of 1-TENG, which suggests that the greater the number of carboxylic acids in the structure of the compound, the greater the TENG performance of the compound. The specific tribological power output properties of compounds 1 and 2 are shown in Fig. S6–S8.†

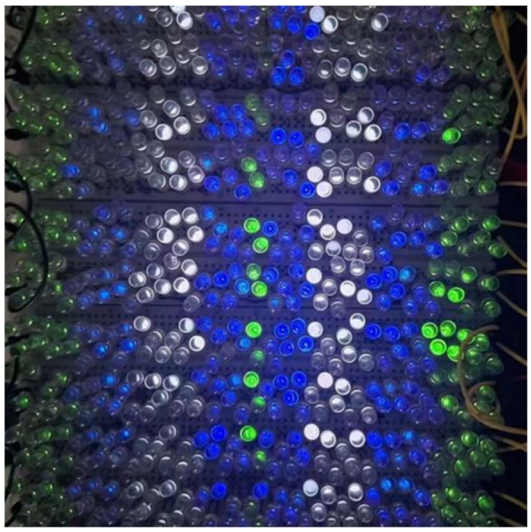

Fig. 7 Lighting a small bulb with 2-TENG lighting the bulb at 5 Hz.

To determine the stability and durability of 2-TENG. We tested the output performance of 2-TENG after 50 000 cycles at 5 Hz and found that the values of I_{sc} and V_{oc} did not show significant changes and were in a stable state (Fig. 5), which indicates that compound 2 has good stability and lays the foundation for its practical application. The output performance of 1-TENG at 5 Hz was also stable (see Fig. S9 and S10†).

To further verify the stability of the friction-generating materials, we observed the morphology of compounds 1–2 and polyvinylidene fluoride (PVDF) by scanning electron microscopy (SEM), and the elemental distributions of compounds 1 and 2 by characteristic K-spectral lines (EDS) (Fig. 6, S11 and S12†). The illustrated results show that the morphology of compounds 1 and 2 remained almost unchanged before and after the experiments, indicating that the compounds are relatively stable.

We used the 2-TENG to light commercial LED lamps at a test frequency of 5 Hz and found that we could successfully light commercial light-emitting diode (LED) lamps (Fig. 7). In conclusion, 2-TENG with high output performance and excellent cycling stability will have a broad application prospect.

Conclusions

In summary, we have synthesized two MOFs with Zn and Cu as metal centers, and H_4TCPE and H_8ETTB as ligands, respectively. Those two materials was used as electrode materials for the preparation of TENG devices by solvent thermogenesis. The current–voltage outputs of Cu-TENG and Zn-TENG were 68.23 μA and 485.32 V, 84.49 μA and 560.45 V, respectively, at 5 Hz frequency, and 50 000 cycles of Cu-TENG were found to have good stability of I_{sc} and V_{oc}, which lays the foundation for future practical applications. Since the metal center has less influence on its performance, but the final performance structure shows that the output performance of Cu-TENG is significantly higher than that of Zn-TENG, this experiment reveals the influence of the structure on its output performance, and the higher the number of carboxylic acids, the higher its performance. It provides a simple method for designing friction nanoelectrode materials in the future.

Conflicts of interest

There are no conflicts to declare.

Acknowledgements

This work was financially supported by Project funded by China Postdoctoral Science Foundation (2021M692907), the National Natural Science Foundation of China (No. 21901264 and 21902189), Young Backbone Teacher of Zhongyuan University of Technology (2020XQG10, 2020XQG09).

Notes and references

1 W. A. Braff, J. M. Mueller and J. E. Trancik, Value of storage technologies for wind and solar energy, *Nat. Clim. Change*, 2016, **6**(10), 964–969.
2 T. Lehtola and A. Zahedi, Solar energy and wind power supply supported by storage technology: a review, *Sustain. Energy Technol. Assess.*, 2019, **35**, 25–31.
3 M. B. Hayat, D. Ali, K. C. Monyake, L. Alagha and N. Ahmed, Solar energy-a look into power generation, challenges, and a solar-powered future, *Int. J. Energy Res.*, 2019, **43**(3), 1049–1067.
4 C. Garcia and I. Trendafilova, Real-time diagnosis of small energy impacts using a triboelectric nanosensor, *Sens. Actuators, A*, 2019, **291**, 196–203.
5 G. Khandelwal, A. Chandrasekhar, N. R. Alluri, V. Vivekananthan, N. P. Maria Joseph Raj and S.-J. Kim, Trash to energy: a facile, robust and cheap approach for mitigating environment pollutant using household triboelectric nanogenerator, *Appl. Energy*, 2018, **219**, 338–349.
6 G. Khandelwal, T. Minocha, S. K. Yadav, A. Chandrasekhar, N. P. Maria Joseph Raj, S. C. Gupta and S.-J. Kim, All edible materials derived biocompatible and biodegradable triboelectric nanogenerator, *Nano Energy*, 2019, **65**, 104016.
7 C. Garcia, I. Trendafilova and J. Sanchez del Rio, Detection and measurement of impacts in composite structures using a self-powered triboelectric sensor, *Nano Energy*, 2019, **56**, 443–453.
8 Y. Li, G. Cheng, Z.-H. Lin, J. Yang, L. Lin and Z. L. Wang, Single-electrode-based rotationary triboelectric nanogenerator and its applications as self-powered contact area and eccentric angle sensors, *Nano Energy*, 2015, **11**, 323–332.
9 S. Hajra, M. Sahu, R. Sahu, A. M. Padhan, P. Alagarsamy, H.-G. Kim, H. Lee, S. Oh, Y. Yamauchi and H. J. Kim, Significant effect of synthesis methodologies of metal-organic frameworks upon the additively manufactured dual-mode triboelectric nanogenerator towards self-powered applications, *Nano Energy*, 2022, **98**, 107253.
10 G. Khandelwal, A. Chandrasekhar, N. P. Maria Joseph Raj and S. J. Kim, Metal–organic framework: a novel material for triboelectric nanogenerator-based self-powered sensors and systems, *Adv. Energy Mater.*, 2019, **9**(14), 1803581.
11 X. He, H. Zou, Z. Geng, X. Wang, W. Ding, F. Hu, Y. Zi, C. Xu, S. L. Zhang, H. Yu, M. Xu, W. Zhang, C. Lu and Z. L. Wang, A hierarchically nanostructured cellulose fiber-based triboelectric nanogenerator for self-powered healthcare products, *Adv. Funct. Mater.*, 2018, **28**(45), 1805540.
12 C. Bu, F. Li, K. Yin, J. Pang, L. Wang and K. Wang, Research progress and prospect of triboelectric nanogenerators as self-powered human body sensors, *ACS Appl. Electron. Mater.*, 2020, **2**(4), 863–878.
13 Z. L. Wang, Triboelectric nanogenerator (TENG)—sparking an energy and sensor revolution, *Adv. Energy Mater.*, 2020, **10**(17), 137–143.
14 Z. Liu, J. Nie, B. Miao, J. Li, Y. Cui, S. Wang, X. Zhang, G. Zhao, Y. Deng, Y. Wu, Z. Li, L. Li and Z. L. Wang, Self-powered intracellular drug delivery by a biomechanical energy-driven triboelectric nanogenerator, *Adv. Mater.*, 2019, **31**(12), e1807795.
15 S. Parandeh, N. Etemadi, M. Kharaziha, G. Chen, A. Nashalian, X. Xiao and J. Chen, Advances in triboelectric nanogenerators for self-powered regenerative medicine, *Adv. Funct. Mater.*, 2021, **31**(47), 2105169.
16 C. Zhao, H. Feng, L. Zhang, Z. Li, Y. Zou, P. Tan, H. Ouyang, D. Jiang, M. Yu, C. Wang, H. Li, L. Xu, W. Wei and Z. Li, Highly efficient *in vivo* cancer therapy by an implantable magnet triboelectric nanogenerator, *Adv. Funct. Mater.*, 2019, **29**(41), 1808640.
17 G. Khandelwal, N. P. Maria Joseph Raj and S.-J. Kim, Triboelectric nanogenerator for healthcare and biomedical applications, *Nano Today*, 2020, **33**, 100882.
18 Q. Niu, L. Huang, S. Lv, H. Shao, S. Fan and Y. Zhang, Pulse-driven bio-triboelectric nanogenerator based on silk nanoribbons, *Nano Energy*, 2020, **74**, 104837.
19 Z. Liu, H. Li, B. Shi, Y. Fan, Z. L. Wang and Z. Li, Wearable and implantable triboelectric nanogenerators, *Adv. Funct. Mater.*, 2019, **29**(20), 1808820.
20 A. Babu, I. Aazem, R. Walden, S. Bairagi, D. M. Mulvihill and S. C. Pillai, Electrospun nanofiber based TENGs for wearable

electronics and self-powered sensing, *Chem. Eng. J.*, 2023, **452**, 1385–8947.

21 S. Cui, Y. Zheng, J. Liang and D. Wang, Triboelectrification based on double-layered polyaniline nanofibers for self-powered cathodic protection driven by wind, *Nano Res.*, 2018, **11**(4), 1873–1882.

22 S. Cui, Y. Zheng, J. Liang and D. Wang, Conducting polymer PPy nanowire-based triboelectric nanogenerator and its application for self-powered electrochemical cathodic protection, *Chem. Sci.*, 2016, **7**(10), 6477–6483.

23 H. Zhang, S. Zhang, G. Yao, Z. Huang, Y. Xie, Y. Su, W. Yang, C. Zheng and Y. Lin, Simultaneously harvesting thermal and mechanical energies based on flexible hybrid nanogenerator for self-powered cathodic protection, *ACS Appl. Mater. Interfaces*, 2015, **7**(51), 28142–28147.

24 Y. Zhang, J. Wu, S. Cui, W. Wei, W. Chen, R. Pang, Z. Wu and L. Mi, Organosulfonate counteranions-a trapped coordination polymer as a high-output triboelectric nanogenerator material for self-powered anticorrosion, *Chemistry*, 2020, **26**(3), 584–591.

25 Z. Shao, J. Chen, K. Gao, Q. Xie, X. Xue, S. Zhou, C. Huang, L. Mi and H. Hou, A double-helix metal-chain metal-organic framework as a high-output triboelectric nanogenerator material for self-powered anticorrosion, *Angew. Chem., Int. Ed. Engl.*, 2022, **61**(40), e202208994.

26 A. Maitra, A. K. Das, R. Bera, S. K. Karan, S. Paria, S. K. Si and B. B. Khatua, An approach to fabricate PDMS encapsulated all-solid-state advanced asymmetric supercapacitor device with vertically aligned hierarchical Zn-Fe-Co ternary oxide nanowire and nitrogen doped graphene nanosheet for high power device applications, *ACS Appl. Mater. Interfaces*, 2017, **9**(7), 5947–5958.

27 Z. Wang, Z. Ruan, Z. Liu, Y. Wang, Z. Tang, H. Li, M. Zhu, T. F. Hung, J. Liu, Z. Shi and C. Zhi, A flexible rechargeable zinc-ion wire-shaped battery with shape memory function, *J. Mater. Chem. A*, 2018, **6**(18), 8549–8557.

28 Y. Liu, J. Mo, Q. Fu, Y. Lu, N. Zhang, S. Wang and S. Nie, Enhancement of triboelectric charge density by chemical functionalization, *Adv. Funct. Mater.*, 2020, **30**(50), 2004714.

29 X. Chen, K. Geng, R. Liu, K. T. Tan, Y. Gong, Z. Li, S. Tao, Q. Jiang and D. Jiang, Covalent organic frameworks: chemical approaches to designer structures and built-in functions, *Angew. Chem., Int. Ed. Engl.*, 2020, **59**(13), 5050–5091.

30 L. Jiao, J. Y. R. Seow, W. S. Skinner, Z. U. Wang and H.-L. Jiang, Metal–organic frameworks: structures and functional applications, *Mater. Today*, 2019, **27**, 43–68.

31 F. Bigdeli, C. T. Lollar, A. Morsali and H. C. Zhou, Switching in metal-organic frameworks, *Angew. Chem., Int. Ed. Engl.*, 2020, **59**(12), 4652–4669.

32 R. Medishetty, V. Nalla, L. Nemec, S. Henke, D. Mayer, H. Sun, K. Reuter and R. A. Fischer, A new class of lasing materials: intrinsic stimulated emission from nonlinear optically active metal–organic frameworks, *Adv. Mater.*, 2017, **29**(17), 1605637.

33 Z. Wei, W. Lu, H. L. Jiang and H. C. Zhou, A route to metal–organic frameworks through framework templating, *Inorg. Chem.*, 2013, **52**(3), 1164–1166.

34 J. Chen, Z. Shao, Y. Zhao, X. Xue, H. Song, Z. Wu, S. Cui, L. Zhang, C. Huang, L. Mi and H. Hou, Metal-ion coupling in metal–organic framework materials regulating the output performance of a triboelectric nanogenerator, *Inorg. Chem.*, 2022, **61**(5), 2490–2498.

35 S. Wang, Y. Xie, S. Niu, L. Lin and Z. L. Wang, Freestanding triboelectric-layer-based nanogenerators for harvesting energy from a moving object or human motion in contact and non-contact modes, *Adv. Mater.*, 2014, **26**(18), 2818–2824.

36 T. Jiang, X. Chen, C. B. Han, W. Tang and Z. L. Wang, Theoretical study of rotary freestanding triboelectric nanogenerators, *Adv. Funct. Mater.*, 2015, **25**(19), 2928–2938.

37 S. Niu, S. Wang, L. Lin, Y. Liu, Y. S. Zhou, Y. Hu and Z. L. Wang, Theoretical study of contact-mode triboelectric nanogenerators as an effective power source, *Energy Environ. Sci.*, 2013, **6**(12), 3576–3583.

38 S. Niu, Y. Liu, S. Wang, L. Lin, Y. S. Zhou, Y. Hu and Z. L. Wang, Theory of sliding-mode triboelectric nanogenerators, *Adv. Mater.*, 2013, **25**(43), 6184–6193.